THE ECLIPSING BINARY CM DRACONIS: A STUDY WITH XMM-NEWTON

M. Güdel[1], A. Telleschi[1], S. L. Skinner[2], M. Audard[3], and J.-U. Ness[4]

[1]Paul Scherrer Institut, Würenlingen and Villigen, CH-5232 Villigen PSI, Switzerland
[2]CASA, University of Colorado, Boulder, CO 80309-0389, USA
[3]Columbia University, 550 W. 120th St., New York, NY 10027, USA
[4]Department of Physics, University of Oxford, 1 Keble Road, Oxford OX1 3NP, UK

Abstract

We present recent XMM-Newton X-ray observations of the eclipsing M dwarf binary CM Draconis (dM4.5, period = 1.27 d, $i = 89.8$ deg), obtained around each of the optical primary and secondary eclipses. The X-ray light curves reveal clear and long (1–2 hours) eclipses of coronal material, additional to some intrinsic X-ray variability. We present a light-curve inversion to determine properties of the 3-D distribution of coronal material. We also discuss the simultaneous U-band light curves obtained with the optical monitor.

Key words: Stars: coronae – Stars: eclipses – Stars: flares – Stars: X-rays – Stars: CM Draconis

1. Introduction

Investigations of stellar coronal X-ray structure are still in an infant state. Only indirect estimates of coronal extent and structure are available for any star other than the Sun. The situation is somewhat better at radio wavelengths where large, ordered magnetic fields have been detected around active and young stars (e.g., Mutel et al. 1985, Beasley & Güdel 2000, Smith et al. 2003). These structures may, however, be different from more compact active regions that comprise hot, X-ray emitting plasma. We present here a preliminary analysis of the X-ray spectra and light curves of the short-period (1.27 d) eclipsing binary CM Draconis, providing geometrical constraints (in longitude, latitude, radial extent) on the location of the plasma, and information on the temperature and density range of the coronal plasma.

2. The CM Draconis binary

CM Dra is one of the rare, fully eclipsing late-type main-sequence binaries. It consists of two very similar dM4.5e stars. A comparison with the better studied eclipsing binary YY Gem (Güdel et al. 2001) is instructive. Table 1 summarizes properties of both binary systems.

The CM Dra system is outstanding as its fundamental parameters are among the best determined of any stellar system. It shows well-expressed optical eclipses every 0.63 d, with a depth of 0.8 mag and a duration of 1.5 hrs each (Fig. 1).

Table 1. Properties of the CM Dra system and comparison with YY Gem.

	CM Dra	YY Gem
Distance [pc]	14.7[a]	15.8[b]
Spectrum	dM4.5e[c]	dM1e[d]
Radii [$R_\odot$]	0.25, 0.23[e]	0.66, 0.58[f]
Masses [$M_\odot$]	0.23, 0.21[g]	0.62, 0.57[h]
Separation [$R_\odot$]	3.74[i]	3.8[j]
log$L_{\rm X}$ [erg s^{-1}]	28.5[k]	29.5[l]
Period [d]	1.27[m]	0.81[n]
Inclination [deg]	89.82[o]	86.2[p]

REFERENCES: *a* Perryman et al. (1997) (Castor); *b* Harrington & Dahn (1980); *c* Deeg et al. (1998); *d* Joy & Abt (1974); *e* Lacy (1977), Metcalfe et al. (1996); *f* Haisch et al. (1990); *g* Metcalfe et al. (1996) (Lacy 1977); *h* Bopp (1974), Haisch et al. (1990); *i* Lacy (1977), Metcalfe et al. (1996); *j* Bopp (1974), Haisch et al. (1990); *k* this work; *l* Güdel et al. (2001); *m* Lacy (1977), Metcalfe et al. (1996); *n* Bopp (1974); *o* Lacy (1977); *p* Pettersen (1976).

3. Observations with XMM-Newton

XMM-Newton observed CM Dra around a secondary eclipse and, 1.9 days later, during a primary eclipse (Fig. 1). Each observation lasted for ≈23 ks. All detectors were fully operational. Both X-ray eclipses are well developed although the light curves show considerable additional modulation, including X-ray and concurrent U-band flares. There are, however, only modest changes in the hardness ratio (count rate above 1 keV/count rate below); part of the modulation may be due to rotation as active regions move into and out of sight.

A closer investigation of the U-band and X-ray flares (see Fig. 2) shows some of the former to characteristically precede the more gradual X-ray flares. This is expected from the analogy with solar flares: white-light flares are interpreted as being due to the initially accelerated electrons upon collision in the chromosphere. The plasma is thereby heated and gradually fills coronal loops, subsequently cooling by emission of X-rays.

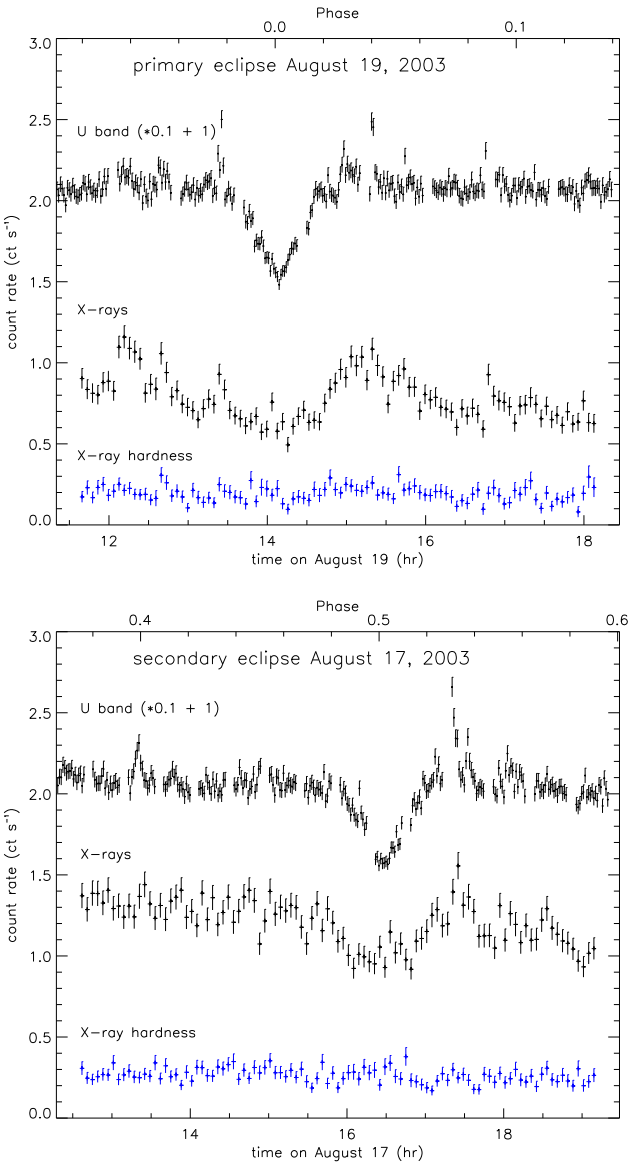

Figure 1. XMM-Newton light curves of CM Dra's primary (top) and secondary eclipse (bottom). The three curves in each panel refer to, from top to bottom, the U-band filter of the OM instrument (bin size = 80 s) where the count rate was divided by ten and subsequently shifted by +1 ct s^{-1} for illustration purposes; the combined EPIC X-ray curve (bin size = 240 s); and the spectral hardness.

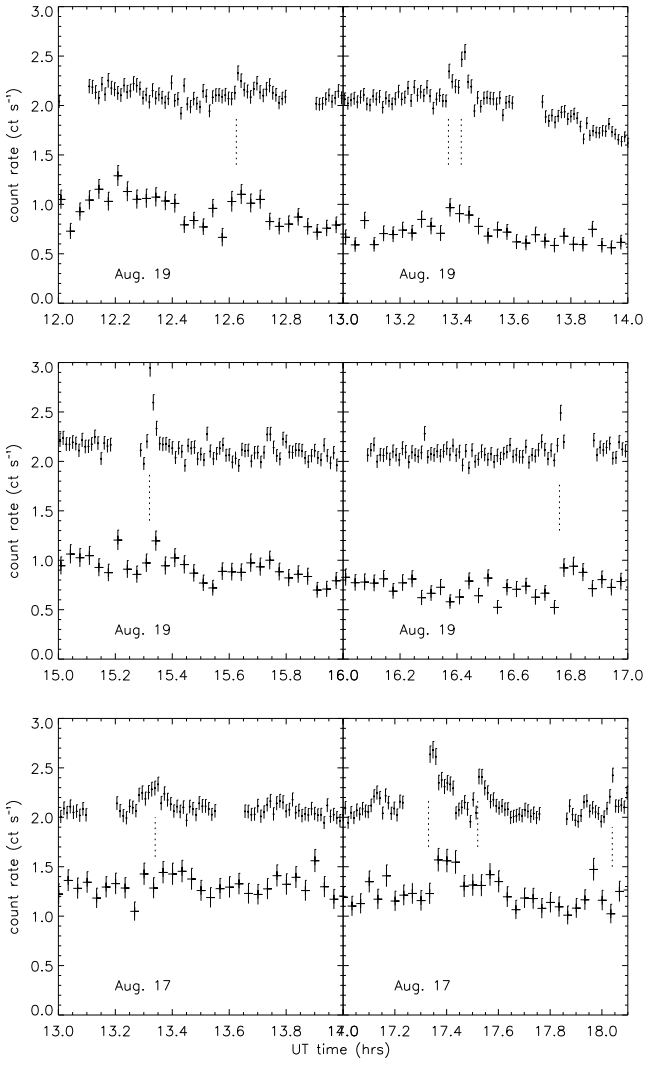

Figure 2. Extracts of the light curves (upper curve in each panel: U band, multiplied and shifted, at 40 s resolution; lower curve: X-rays at 120 s resolution), with optical flares marked by vertical dotted lines.

4. Spectra and emission measure distribution

Line-dominated regions of the RGS spectra (Fig. 3; Table 2) and the high-energy tail of the MOS spectrum were fitted in SPEX (using the method described by Audard et al. 2003). The resulting DEM (Fig. 4; without error bars in this preliminary version) shows a dominant component around 10 MK. We find [Ne/Fe] $\approx$ 0.9 and [O/Fe] $\approx$ 1.0 (logarithmic notation, relative to solar photospheric abundances of Anders & Grevesse 1989).

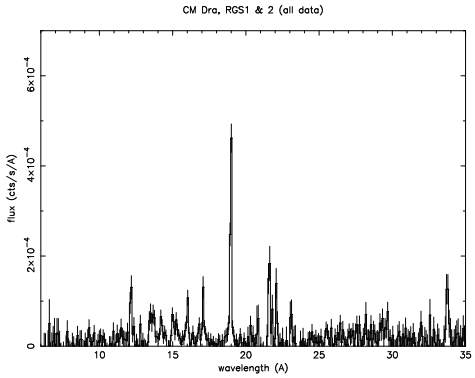

Figure 3. Average RGS spectrum, summing all available data from both observations.

Table 2. Line fluxes in summed RGS 1&2 spectra (both observations) obtained with Lorentzian templates of given FWHM.

λ [Å]	FWHM [Å]	flux $[10^{-14}\mathrm{erg/cm^2/s}]$
12.141 ± 0.0147	0.0798	4.3032 ± 1.3655
13.464 ± 0.0505	0.1604	2.8028 ± 1.5039
13.716 ± 0.0602	0.1604	2.7003 ± 1.4924
14.220 ± 0.0608	0.1604	2.5891 ± 1.3610
15.019 ± 0.0246	0.0779	2.1204 ± 0.9668
15.281 ± 0.0387	0.0779	1.4609 ± 0.9129
16.001 ± 0.0249	0.1095	2.9001 ± 1.0972
16.771 ± 0.0438	0.1095	1.2016 ± 0.9186
17.070 ± 0.0277	0.1095	2.8207 ± 1.0408
18.617 ± 0.0905	0.0710	0.3748 ± 0.6150
18.970 ± 0.0096	0.0710	8.2786 ± 1.1871
20.849 ± 0.0732	0.0800	0.6639 ± 0.5099
21.592 ± 0.0107	0.0800	3.5247 ± 0.8467
21.801 ± 0.0366	0.0800	0.6770 ± 0.6250
22.081 ± 0.0171	0.0800	2.0464 ± 0.7111
23.091 ± 0.0292	0.0800	1.0577 ± 0.6100
24.488 ± 0.0415	0.0800	0.5744 ± 0.5359
25.495 ± 0.0407	0.0800	0.6502 ± 0.5339
28.207 ± 0.0272	0.0800	0.9393 ± 0.5106
29.194 ± 0.0271	0.0800	0.8392 ± 0.4976
29.684 ± 0.0334	0.0800	0.9332 ± 0.4918
33.745 ± 0.0133	0.0800	1.8392 ± 0.5199
34.458 ± 0.0423	0.0800	0.4854 ± 0.3850

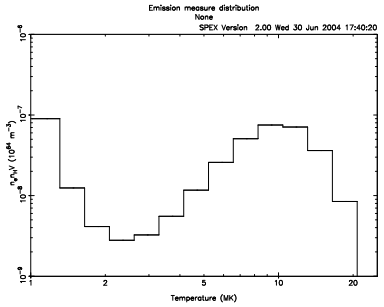

Figure 4. Emission measure distribution derived from the spectrum obtained on Aug. 17.

5. Coronal structure from eclipses

We have applied a light-curve inversion algorithm previously described by Siarkowski (1992) (for AR Lac) and Güdel et al. (2001) (for YY Gem). There is considerable uncertainty in the coronal structure inferred from the X-ray light curves because of limited time coverage, intrinsic flare-like variability, and our assumption of the absence of changes in coronal structure between the two observations. We eliminated possible flares (around 12:15, 12:45, 13:30, and 15 UT in the Aug. 19 observation, and around 17:30 in the Aug. 17 observation) before applying the algorithm. Our results will thus only provide some overall constraints on the large-scale structure of the coronae. Six phases of our solution are shown in Fig. 5.

We analyzed these 3-D distributions further, presenting results for the entire corona and for a region within ± 45 deg in longitude and ± 60 deg in latitude of the points

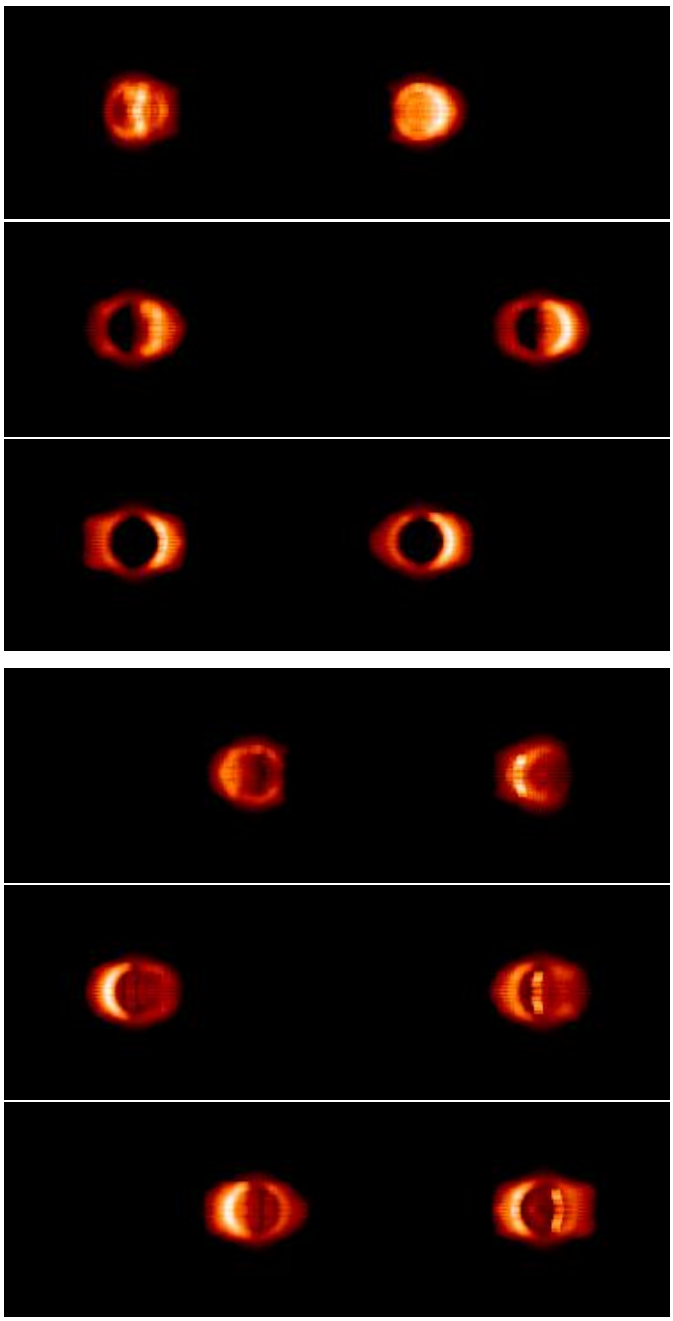

Figure 5. Reconstructed coronal structure, for phases of 45, 90 and 135 degrees (upper three panels, primary star at left), and for 225, 270, and 315 degrees (primary star at right).

that are centrally eclipsed; these are the regions that are best constrained by our eclipse image reconstruction. The following properties characterize the reconstructions:

- The distributions of emission measure in latitude and longitude are shown in Figs. 6. Much of the plasma is seen at intermediate latitudes, but the distribution in longitude is very inhomogeneous.
- The average radial density profile (Fig. 7) shows a scale height of approximately $(1 \pm 0.1) \times 10^{10}$ cm (except for

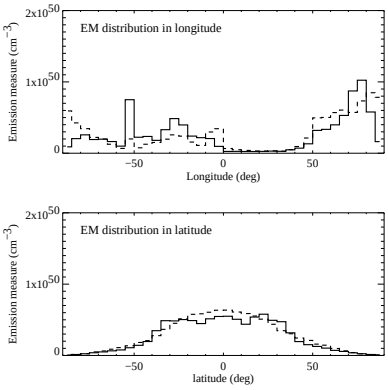

Figure 6. Distribution of emission measure in longitude (upper plot) and in latitude (lower plot), for the primary (solid histogram) and the secondary (dashed).

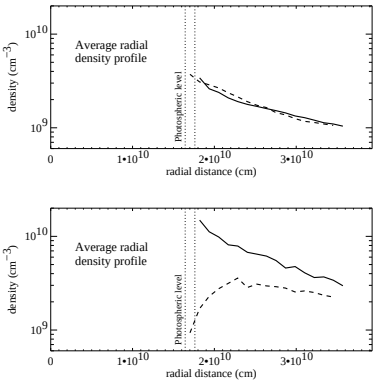

Figure 7. Radial density profile from coronal reconstruction. Upper plot: for the entire corona; lower plot: for constrained volume. Solid line: primary; dashed line: secondary.

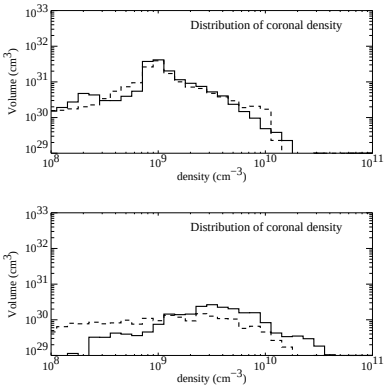

Figure 8. Volume occupation by different densities. Panels and line styles as in Fig. 7.

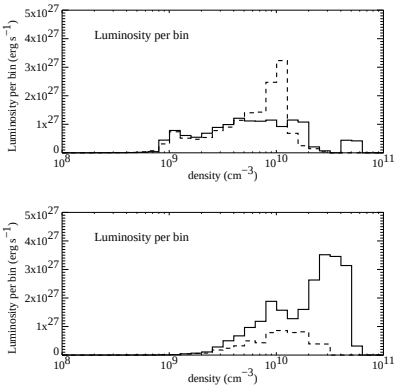

Figure 9. Contributions of volumes of different densities to the X-ray luminosities of the two stars, assuming equal temperatures. Panels and line styles as in Fig. 7.

the constrained analysis of the secondary). This corresponds to an isothermal coronal plasma of ≈ 8 MK, in the midst of the dominant plasma temperatures found from the spectra.

– Most of the plasma resides at densities between $10^9 - 10^{10}$ cm^{-3} (Fig. 8); such densities are reminiscent of densities of solar active regions.
– However, when calculating the contributions of these volume elements to the X-ray emission (Fig. 9), a considerable fraction is due to densities $> 10^{10}$ cm^{-3}; this would be marginally detected in the O VII He-like triplet. However, the latter refers exclusively to cool plasma. The RGS O VII data did not reveal strong evidence for high densities.

Acknowledgements

Financial support from the Swiss NSF (grant 20-66875.01) is acknowledged. XMM-Newton is an ESA mission funded by ESA member states and the USA.

References

Anders, E., Grevesse, N. 1989, Geochim, Cosmochim. Acta, 53, 197

Audard, M., Güdel, M., Sres, A., Raassen, A. J. J., Mewe, R. 2003, A&A, 398, 1137

Beasley, A.J., & Güdel, M. 2000, ApJ, 569, 961

Bopp, B. W. 1974, ApJ, 193, 389

Deeg, H. J., Doyle, L. R., Kozhevnikov, V. P., Martin, E. L., Oetiker, B., et al. 1998, A&A, 338, 479

Güdel, M., Audard, M., Magee, H., Franciosini, E., Grosso, N., et al. 2001, A&A, 365, L344

Haisch, B. M., Schmitt, J. H. M. M., Rodonò, M., Gibson, D. M. 1990, A&A, 230, 419

Harrington, R. S., Dahn, C. C. 1980, AJ, 85, 454

Heintz, W. D. 1988, PASP, 100, 834

Joy, A. H., Abt, H. A. 1974, ApJS, 28, 1

Lacy, C.H. 1977, ApJ, 218, 444

Metcalfe, T. S., Mathieu, R. D., Latham, D. W., Torres, G. 1996, ApJ, 456, 356

Mutel, R. L., Lestrade, J. F., Preston, R. A., Phillips, R. B. 1985, ApJ, 289, 262

Perryman, M. A. C., and the *Hipparcos* Science Team 1997, The *Hipparcos* and *Tycho* Catalogues (ESA SP-1200)

Pettersen, B. R. 1976, Catalogue of Flare Star Data, Rept. 46, Univ. Of Oslo

Siarkowski, M. 1992, MNRAS, 259, 453

Smith, K., Pestalozzi, M., Güdel, M., Conway, J., Benz, A. O. 2003, A&A, 406, 957